Accepted Manuscript

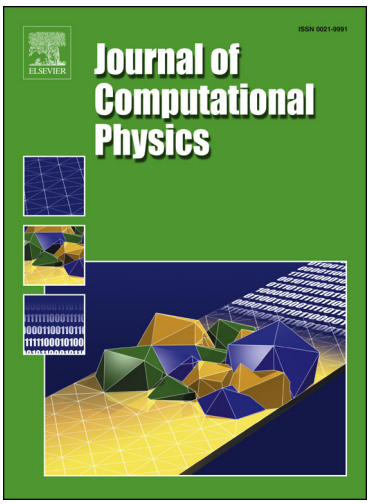

Modified sequential fully implicit scheme for compositional flow simulation

A. Moncorgé, H.A. Tchelepi, P. Jenny

PII: S0021-9991(17)30125-0
DOI: http://dx.doi.org/10.1016/j.jcp.2017.02.032
Reference: YJCPH 7163

To appear in: *Journal of Computational Physics*

Received date: 11 July 2016
Revised date: 31 January 2017
Accepted date: 11 February 2017

Please cite this article in press as: A. Moncorgé et al., Modified sequential fully implicit scheme for compositional flow simulation, *J. Comput. Phys.* (2017), http://dx.doi.org/10.1016/j.jcp.2017.02.032

Modified Sequential Fully Implicit Scheme for Compositional Flow Simulation

A. Moncorgé [a,*], H.A. Tchelepi[b], P. Jenny[c]

[a] *TOTAL E&P UK, Geoscience Research Center, Aberdeen, UK.*
[b] *Energy Resources Engineering Department, Stanford University, Stanford, California.*
[c] *Institute of Fluid Dynamics, ETH Zurich, Zurich, Switzerland.*

Abstract

The fully implicit (FI) method is widely used for numerical modeling of multiphase flow and transport in porous media. The FI method is unconditionally stable, but that comes at the cost of a low-order approximation and high computational cost. The FI method entails iterative linearization and solution of fully-coupled linear systems with mixed elliptic/hyperbolic character. However, in methods that treat the near-elliptic (flow) and hyperbolic (transport) separately, such as multiscale formulations, sequential solution strategies are used to couple the flow (pressures and velocities) and the transport (saturations/compositions). The most common sequential schemes are: the implicit pressure explicit saturation (IMPES), and the sequential fully implicit (SFI) schemes. Problems of practical interest often involve tightly coupled nonlinear interactions between the multiphase flow and the multicomponent transport. For such problems, the IMPES approach usually suffers from prohibitively small timesteps in order to obtain stable numerical solutions. The SFI method, on the other hand, does not suffer from a temporal stability limit, but the convergence rate can be extremely slow. This slow convergence rate of SFI can offset the gains obtained from separate and specialized treatments of the flow and transport problems. In this paper, we analyze the nonlinear coupling between flow and transport for compressible, compositional systems with complex interphase mass transfer. We isolate the nonlinear effects related to transmissibility and compressibility from those due to interphase mass transfer, and we propose a modified SFI (m-SFI) method. The new scheme involves enriching the 'standard' pressure equa-

*Corresponding author arthur.moncorge@total.com

tion with coupling between the pressure and the saturations/compositions. The modification resolves the convergence problems associated with SFI and provides a strong basis for using sequential formulations for general-purpose simulation. For a wide parameter range, we show that the proposed m-SFI algorithm is as robust as the FI method with a comparable convergence rate.

Keywords: nonlinear dynamics, numerical flow simulation, sequential implicit, operator splitting, coupled flow and transport, multiscale methods, flow in porous media, compositional formulation, multiphase flow, multi-component transport, compositional reservoir simulation

---

Contents

1 Introduction **3**

2 Modified Sequential Fully Implicit (m-SFI) Scheme **5**
- 2.1 Natural-Variables Compositional Formulation 5
- 2.2 Nonlinear FI and SFI Solvers 7
- 2.3 CFL Limit for Explicit Treatment of Thermodynamics 9
- 2.4 m-SFI Algorithm 11

3 Numerical Experiments and Discussion **18**
- 3.1 Depletion Test Cases 19
- 3.2 Re-Compression Test Cases 21
- 3.3 Realistic Case 24

4 Conclusions **24**

5 Nomenclature **27**

6 Acknowledgments **28**

7 Appendix A: Description of the Models **28**

8 Appendix B: Stability Analysis **31**

9 Appendix C: SI Metric Conversion Factors **32**

10 References **33**

1. Introduction

There has been growing interest in multiscale formulations for modeling flow and transport processes to manage subsurface water and hydrocarbon resources, and the sequestration of CO_2. Multiscale finite element (MSFE) methods have been first proposed by [18, 3, 7, 1]. Subsequently, Jenny et al. [19] proposed the multiscale finite-volume method (MSFV). The original MSFV approach deals with the flow (pressure and total velocity) in a multiscale manner, while the transport (saturations) problem is usually solved on the reference fine grid. The method has been extended to account for compressibility and buoyancy effects and for multiscale treatment of the transport problem [20, 47] as well as recent works addressing real reservoir geometries [32, 33, 26] but the developments have not reached the level of general-purpose utility.

In compositional reservoir simulation, the interphase mass transfer can often be captured by the so-called black-oil formulation, where the chemical equilibrium between the hydrocarbon liquid and vapor fluid phases is expressed as a function of pressure [4]. For most enhanced oil-recovery (EOR) processes, however, the interphase mass transfer requires more complex treatment using equilibrium ratios (K-values), or cubic equations-of-state (EOS) [21, 16, 10, 34, 46, 2, 45]. EOS-based compositional formulations differ - mainly - in the splitting of the unknowns (degrees-of-freedom) into primary and secondary sets. For detailed descriptions and comparisons of the different compositional formulations, we refer to [5, 44]. The MSFV framework has been extended to black-oil [24, 33] and recently to compositional multicomponent two-phase problems [17].

The mathematical properties of the flow problem (near-elliptic pressure equation) are very different from those of the transport problem (near-hyperbolic saturation/composition equations). The different characters of the flow and transport problems provide an opportunity to use different (specialized) discretization schemes and solution methods. Sequential strategies were originally developed to be able to simulate reservoir models that were too large - in terms of numbers of cells and number of components - for the fully implicit (FI) solution scheme. The simplest sequential strategies are based on the implicit pressure explicit saturation (IMPES) approach [38, 41, 4, 11]. The explicit treatment of the transport problem in IMPES schemes leads to limits on the timestep that can be used [13]; these stability limits can be quite severe for highly detailed heterogeneous reservoir models. To help deal with

these restrictions, sequential-implicit methods were introduced for immiscible multiphase 'coning' problems [28, 35] and then extended to black-oil [40, 22] and compositional formulations [45]. The sequential implicit (SI) formulation of Watts consists of a pressure solution step, in which IMPES pressure equation is solved followed by implicit solution of the transport whereby the total-velocity field is fixed. One SI iteration is computationally more efficient than a fully implicit (FI) iteration. SI methods are more stable than IMPES methods, but they suffer from conditional stability due to the semi-implicit treatment of the velocity. In addition, in SI schemes, material balance errors may accumulate with time, especially for three-phase systems. In [45], a special treatment is introduced to control the material balance by accounting for the volume discrepancy from the previous timestep at the beginning of the next one. The sequential fully implicit (SFI) method was proposed for the MSFV method by Jenny et al. [20]. The SFI scheme leads to the same numerical solution of the FI method; thus, it is consistent and mass conservative. The SFI algorithm consists of an outer loop for the coupled system of flow and transport, and an inner loop. The inner loop is made up of two loops performed in sequence: one for the pressure equation and one for the saturations/compositions. The SFI scheme is quite efficient compared with the FI method for a wide range of problems in which the interphase mass transfer is weakly coupled to the flow problem. For EOR problems with tightly coupled nonlinear interactions due to complex interphase mass transfer, the SFI scheme suffers from convergence difficulties that translate into large numbers of outer iterations and/or smaller timesteps compared with the FI method [25]. In this paper, we analyze the nonlinear coupling between multiphase flow and multi-component transport for systems that involve complex interphase mass transfer in heterogeneous reservoir models, and we propose a modified SFI (m-SFI) method. The modification complements the 'standard' pressure equation with local pressure-saturations/compositions coupling terms. We show across a wide parameter range that the m-SFI algorithm has convergence properties that are similar to, and sometimes even better than, those of the FI method. Compositional fluids with two, six, and eleven components are considered. Formulations based on K-values and equations of state (EOS) were tested for both depletion and recompression test cases with interphase mass transfer and crossing of the phase boundaries.

2. Modified Sequential Fully Implicit (m-SFI) Scheme

In this section, the compositional formulation based on the natural variables for both FI and SFI nonlinear solution algorithms are introduced. Then, criteria that measure the degree of coupling between the pressure and the other variables are derived. These criteria motivate the new m-SFI method.

2.1. Natural-Variables Compositional Formulation

The generalized compositional formulation is our target. The formulation accounts for compressible gas-oil flow with gravity and capillary-pressure effects. In this study, we ignore water that does not exchange mass with the hydrocarbon phases. There are n_h hydrocarbon components, and the natural-variables formulation [10] is employed. For the flow of two hydrocarbon phases, there are $2n_h + 4$ unknowns. They are the gas-phase pressure, P_g, oil-phase pressure, P_o, the saturation of each phase (S_g and S_o), and the mass fractions, y_c and x_c of each hydrocarbon component c in the gas and oil phases, respectively. For the $2n_h + 4$ unknowns, $2n_h + 4$ equations are required. The conservation of hydrocarbon component, c, can be written as

$$\frac{\partial}{\partial t}\left[\phi(y_c\rho_g S_g + x_c\rho_o S_o)\right] + \nabla\cdot\left[y_c\rho_g u_g + x_c\rho_o u_o\right] = q_c, \tag{1}$$

where ρ_g and ρ_o are the fluid-phase mass densities, ϕ the porosity, and q_c a source term. The velocity of each phase $p \in \{g, o\}$ is given by Darcy's law:

$$u_p = -\frac{k_{r_p}}{\mu_p} K\nabla\left(P_p - \rho_p g D\right), \tag{2}$$

where K is the rock permeability, k_{r_p} the relative permeability of each phase, μ_p the phase viscosities, g the gravitational acceleration, and D the depth.

In addition to the n_h conservation equations, n_h+4 local constraint equations are needed to close the system. These include:

$$\sum_{c=1}^{n_h} y_c = 1 \tag{3}$$

$$\sum_{c=1}^{n_h} x_c = 1 \tag{4}$$

$$S_g + S_o = 1. \tag{5}$$

We also have the capillary-pressure-saturation relationship:

$$P_c(S_g) = P_g - P_o \tag{6}$$

where P_c is the capillary pressure. The remaining constraints represent the thermodynamic phase equilibrium for each component (n_h equations). These local equilibrium constraints are enforced only when both gas and oil hydrocarbon phases are present in the control volume. Three different models for the phase equilibrium are used in the reservoir simulation community. The simplest formulation is the black-oil model, which accounts for two hydrocarbon components, whereby the phase compositions are direct functions of the (gas-phase) pressure; that is,

$$y_c = y_{c_{sat}}(P_g) \tag{7}$$

$$x_c = x_{c_{sat}}(P_g). \tag{8}$$

The second model is the K-value compositional formulation, which accounts for many hydrocarbon components. The equilibrium is represented by correlations [14]

$$y_c = K_c(P_g)\, x_c. \tag{9}$$

Finally, the most general formulations are based on the Peng-Robinson [36], Redlich-Kwong [37] and Soave-Redlich-Kwong [39] cubic equations of state (EOS) models. The general approach can be written as [29]

$$\hat{f}_{c,g}(P_g, y_1, ..., y_{n_h}) = \hat{f}_{c,o}(P_g, x_1, ..., x_{n_h}). \tag{10}$$

We have a nonlinear system that consists of $2n_h+4$ equations and $2n_h+4$ unknowns. In [10], the n_h component equations are called 'primary equations', and the remaining $n_h + 4$ local constraint equations are referred as 'secondary equations'. The secondary equations involve variables of a given control-volume (cell) only, and they are used to algebraically eliminate n_h+4 variables. The set of n_h primary variables is sufficient to compute the remaining secondary variables. The pressure P_g of the gas phase is always a primary variable. The remaining $n_h - 1$ primary variables depend on the phase-state of the system. For oil-only cells, the primary component variables are: x_1 to x_{n_h-1}; for gas-only cells, the primary set is: y_1 to y_{n_h-1}, and for cells with both gas and oil phases, the variables are: S_g and y_2 to y_{n_h-1}. The sum of all the component conservation equations (1) gives:

$$\frac{\partial}{\partial t}\left[\phi(\rho_g S_g + \rho_o S_o)\right] + \nabla \cdot \left[\rho_g u_g + \rho_o u_o\right] = q, \tag{11}$$

which is the equation for total-mass conservation. We use this equation in place of one of the component conservations equations, which here is the 'heaviest' hydrocarbon component. The total-mass conservation equation serves as the 'pressure equation', and it has near-elliptic behavior. The component conservation equations, on the other hand, have a near-hyperbolic behavior.

2.2. Nonlinear FI and SFI Solvers

We use a finite-volume method for spatial discretization and a first-order implicit (backward Euler) scheme is used for time. First-order spatial derivatives are discretized using single-point upstream weighting, and second-order spatial derivatives are discretized using a central scheme. In the following, the subscript "P" refers to the pressure equation, or the gas-phase pressure, and subscript "C" refers to the component equations, or the primary component variables. After linearization, one obtains the following coupled linear system:

$$\begin{pmatrix} A_{PP} & A_{PC} \\ A_{CP} & A_{CC} \end{pmatrix} \begin{pmatrix} \delta P \\ \delta C \end{pmatrix} = - \begin{pmatrix} R_P \\ R_C \end{pmatrix}, \tag{12}$$

where $(R_P, R_C)^T$ is the residual vector.

Algorithm 1 describes the FI method, in which ϵ denotes the convergence tolerance.

compute R_P and R_C
while $max(|R_P|, |R_C|) > \epsilon$ **do**
  compute A_{PP}, A_{PC}, A_{CP}, A_{CC}
  compute $\begin{pmatrix} \delta P \\ \delta C \end{pmatrix} = - \begin{pmatrix} A_{PP} & A_{PC} \\ A_{CP} & A_{CC} \end{pmatrix}^{-1} \begin{pmatrix} R_P \\ R_C \end{pmatrix}$
  $P = P + \delta P$
  $C = C + \delta C$
  compute phase-split
  recompute R_P and R_C
end

Algorithm 1: FI method

This algorithm, however, is not a 'true' Newton-Raphson method. This is because the local (equilibrium) constraint equations can change from one iteration to the next due to the appearance, or disappearance, of a fluid

phase. Note that the equilibrium constraint equations are only enforced if both fluid-phases are present. At the end of an iteration, the saturations and mass fractions are restricted to remain in the physical space (i.e., between zero and one). When the saturation of a phase becomes negative, then in addition to setting its value to zero, we assume that the fluid-phase has disappeared. After updating the variables, a phase-split (phase stability) test is performed. To smooth out discontinuities due to variable switching between iterations when a new fluid phase appears, the saturation of that phase is set to a very small value (e.g., 0.001) [10]. This allows the next Newton iteration to lead the system to the correct solution. Obviously, this phase-split (stability) test is required only for single-phase cells.

The SFI method was introduced along with the development of the MSFV method [19, 20]. The SFI scheme sequentially solves the near-elliptic pressure equation and then near-hyperbolic transport equations as described by algorithm 2, in which ϵ, ϵ_P, and ϵ_C are convergence tolerances.

compute R_P and R_C
while $max(|R_P|, |R_C|) > \epsilon$ **do**
  while $|\delta P| > \epsilon_P$ **do**
    compute A_{PP} and R_P
    compute $\delta P = -A_{PP}^{-1} \cdot R_P$
    $P = P + \delta P$
    compute phase-split
  end
  compute total velocity u_t
  while $|\delta C| > \epsilon_C$ **do**
    compute A_{CC} and R_C
    compute $\delta C = -A_{CC}^{-1} \cdot R_C$
    $C = C + \delta C$
    compute phase-split
  end
  recompute R_P and R_C
end

Algorithm 2: SFI method

The SFI method can be efficient for many problems; however, when the coupling between the flow and transport is too strong, the SFI method often requires many more Newton iterations and/or much smaller timesteps

compared with the FI method.

2.3. CFL Limit for Explicit Treatment of Thermodynamics

We derive criteria for the degree of coupling across pressure, saturations, and compositions. We study how errors in the pressure impact the other variables, especially in the presence of interphase mass transfer. We derive Courant-Friedrichs-Lewy (CFL) numbers for the saturations and compositions. These CFL numbers give an indication of the degree of the coupling strength across pressure, saturation, and composition when a sequential (explicit) solution algorithm is employed.

First, we derive the CFL number for explicit treatment of saturation in one-dimension (x). The fractional-flow is given by:

$$f_g = \frac{\lambda_g}{\lambda_t}\left(1 + \frac{\lambda_o}{u_t} K \frac{\partial(\rho_g - \rho_o) g D}{\partial x}\right) \approx \frac{\lambda_g}{\lambda_t}\left(1 + \frac{\lambda_o(\rho_g - \rho_o)}{u_t} g K \frac{\partial D}{\partial x}\right) \tag{13}$$

and the gas-phase velocity can be written as:

$$u_g = f_g u_t - \frac{\lambda_g \lambda_o}{\lambda_t} K \frac{\partial P_c}{\partial x} \tag{14}$$

with the mobility $\lambda_p = \frac{k_{rp}}{\mu_p}$ of each phase $p \in \{g, o\}$. The total-mobility is $\lambda_t = \lambda_g + \lambda_o$, the total-velocity is $u_t = u_g + u_o$, and the fractional-flow and the velocity of the oil phase are, respectively, $f_o = 1 - f_g$ and $u_o = u_t - u_g$. Assuming a constant ϕ, neglecting the spatial gradient $\frac{\partial u_t}{\partial x}$ and the cross-derivatives in the linearized pressure equation, one obtains:

$$\frac{\partial S}{\partial t} = -a_t^S \frac{\partial S}{\partial x} + d^S \frac{\partial^2 S}{\partial x^2} - \frac{\frac{\partial}{\partial P}\left(\rho_g f_g + \rho_o f_o\right)}{\rho_g - \rho_o} \frac{u_t}{\phi} \frac{\partial P}{\partial x} \tag{15}$$

with $S = S_g$, $S_o = 1 - S$,

$$a_t^S = \frac{\partial f_g}{\partial S_g} \frac{u_t}{\phi} \geq 0 \tag{16}$$

and

$$d^S = \frac{\lambda_g \lambda_o}{\lambda_t} \frac{K}{\phi} P_c' \geq 0. \tag{17}$$

Defining the phase-split function $F^S(P, z) = S_g$ with z as the global mass-fraction for each component, we approximate $\frac{\partial P}{\partial x} \approx \left[\frac{\partial F^S}{\partial P}\right]^{-1} \frac{\partial S}{\partial x}$, which leads

to an equation for the derivatives of S; that is,

$$\frac{\partial S}{\partial t} = -a_t^S \frac{\partial S}{\partial x} + d^S \frac{\partial^2 S}{\partial x^2} - a_f^S \frac{\partial S}{\partial x} \tag{18}$$

with

$$a_f^S = \frac{\frac{\partial}{\partial P}\left(\rho_g f_g + \rho_o f_o\right)}{\rho_g - \rho_o} \left[\frac{\partial F^S}{\partial P}\right]^{-1} \frac{u_t}{\phi} \geq 0. \tag{19}$$

This is the standard saturation equation with an additional term that accounts for phase transitions. Discretizing equation (18) with the space and time increments δx and δt, and performing a Neumann stability analysis leads to the CFL number for the explicit treatment of the thermodynamics term but the implicit treatment of the advection and diffusion terms (CFL saturation "flash", ie CFL_{SF}):

$$CFL_{SF} = \left| \frac{2a_f^S \frac{\delta t}{\delta x} - 1}{2a_t^S \frac{\delta t}{\delta x} + 4d^S \frac{\delta t}{\delta x^2} + 1} \right| \tag{20}$$

and the usual CFL number for the explicit treatment of the advection and the diffusion terms (CFL saturation CFL_S):

$$CFL_S = \delta t \left| a_t^S \frac{1}{\delta x} + 2d^S \frac{1}{\delta x^2} \right|. \tag{21}$$

These equations are derived in Appendix B.

We now derive the CFL number for explicit treatment of the compositions. With constant ϕ, neglecting the spatial gradient $\frac{\partial u_t}{\partial x}$ and the cross-derivatives in the linearization of component c equation (1), one obtains for one-dimension flow:

$$\frac{\partial x_c}{\partial t} = -\frac{K_c \rho_g f_g + \rho_o f_o}{K_c \rho_g S_g + \rho_o S_o} \frac{u_t}{\phi} \frac{\partial x_c}{\partial x} - \frac{\frac{\partial}{\partial P}\left(K_c \rho_g f_g + \rho_o f_o\right)}{K_c \rho_g S_g + \rho_o S_o} x_c \frac{u_t}{\phi} \frac{\partial P}{\partial x} \tag{22}$$

with $y_c = K_c x_c$. Defining the phase-split function $F^c(P, z) = x_c$, we approximate $\frac{\partial P}{\partial x} \approx \left[\frac{\partial F^c}{\partial P}\right]^{-1} \frac{\partial x_c}{\partial x}$, and one obtains an equation with only derivatives of x_c; that is,

$$\frac{\partial x_c}{\partial t} = -a_t^c \frac{\partial x_c}{\partial x} - a_f^c \frac{\partial x_c}{\partial x} \tag{23}$$

with

$$a_t^c = \frac{y_c \rho_g f_g + x_c \rho_o f_o}{y_c \rho_g S_g + x_c \rho_o S_o} \frac{u_t}{\phi} \tag{24}$$

and

$$a_f^c = \frac{y_c \frac{\partial(\rho_g f_g)}{\partial P} + x_c \frac{\partial(\rho_o f_o)}{\partial P}}{y_c \rho_g S_g + x_c \rho_o S_o} x_c \left[\frac{\partial F^c}{\partial P}\right]^{-1} \frac{u_t}{\phi}. \tag{25}$$

This is the standard compositional balance, but with an additional term accounting for phase transition effects. This equation is used to obtain the CFL numbers (stability limits) due to phase-transition (CFL composition "flash", ie CFL_{XF}) and flow (CFL composition CFL_X), respectively. The results are:

$$CFL_{XF} = \left|\frac{2a_f^c \frac{\delta t}{\delta x} - 1}{2a_t^c \frac{\delta t}{\delta x} + 1}\right| \tag{26}$$

$$\text{and } CFL_X = \delta t \left|a_t^c \frac{1}{\delta x}\right|. \tag{27}$$

Note that the maximum values refers to those obtained over all the components in the system. A physical argument for these criteria is the following: if we have a gas-oil cell at equilibrium, and a light component is injected, then the pressure and the gas saturation will start to increase. If, on the contrary, a heavy component is injected, then the pressure and gas saturation of the cell will decrease. Thus, depending on the composition entering the cell, the pressure can go up or down, so that changes in the pressure and saturation/compositions are tightly coupled. If the model has several cells, then the problem is more complicated. The CFL_{SF} and CFL_{XF} values are measures of the strength of the pressure-saturation/compositions coupling. When the coupling is small, it means that the pressure will follow the current trend, if the composition content is well approximated. As a result we can decouple pressure from the other variables. When this coupling is strong, then if there is an error in the composition entering the cell, the pressure change can go in the wrong direction.

2.4. m-SFI Algorithm

Here, the modified SFI (m-SFI) approach is described. The pressure update in the FI method (12) can be written as

$$\begin{pmatrix} A_{PP} & A_{PC} \\ A_{CP} & A_{CC} \end{pmatrix} \begin{pmatrix} \delta P \\ \delta C \end{pmatrix} = -\begin{pmatrix} R_P \\ R_C \end{pmatrix} \tag{28}$$

$$P = P + \delta P \tag{29}$$

with δC discarded. Note that A_{PP} is a sparse matrix with scalar elements, whereas A_{CC} is a sparse matrix with block elements of size $(n_h - 1) \times (n_h - 1)$. This pressure update is equivalent to a standard FI iteration; however, computational gains are possible if only the important components of A_{PC} and A_{CC} are considered. Therefore, matrices A_{PCR} and A_{CCR} are introduced, which are approximations of A_{PC} and A_{CC}. A_{PCR} and A_{CCR} are block-diagonal matrices with some off-diagonal blocks for cells with mass transfer between the fluid phases, specifically,

- For cells that currently experience mass transfer between the fluid phases (i.e. cells that have both gas and oil present during the current iteration).
- For cells that have experienced mass transfer between the fluid phases during the current timestep.
- In addition, to limit discontinuities due to removing or adding the coupling terms, for all cells adjacent to those for which one of the first two criteria are met.

We are interested in using timesteps comparable to the FI method. For such compositional simulations, the CFL_{SF} and CFL_{XF} can have very large values during a Newton iteration, and that can destabilize the overall Newton path of a scheme such as the SFI method. Instead of strictly monitoring the various CFL numbers during the iterations for a given timestep, we employed a simple strategy for the m-SFI implementation. A cell that has two phases (gas and oil) during the current iteration retains fully implicit coupling. In order to ensure that no instabilities propagate to a neighboring cell, we retain full implicit coupling to all the neighbors of a two-phase cell. Since most of the cells in a reservoir model are not expected to experience mass transfer between the fluid phases, A_{PCR} and A_{CCR} are likely to be nearly block-diagonal. The m-SFI pressure update is then approximated by

$$\begin{pmatrix} A_{PP} & A_{PCR} \\ A_{CP} & A_{CCR} \end{pmatrix} \begin{pmatrix} \delta P \\ \delta C \end{pmatrix} = - \begin{pmatrix} R_P \\ R_C \end{pmatrix} \tag{30}$$

$$P = P + \delta P. \tag{31}$$

The system associated with the FI procedure for a 2D problem with 10 gridblocks is shown in Figure 1. In sub-plot (a), A_{PP} is dark-blue, A_{PC} is

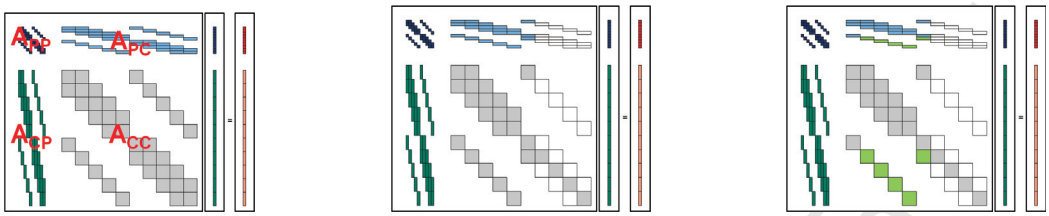

(a) (b) (c)

Figure 1: The systems associated with a 2D problem with 10 gridblocks. (a) shows the FI system; (b) shows the AI system when the last four gridblocks are treated using IMPES. Here, A_{PP} is dark-blue, A_{PC} is light-blue, A_{CP} is green, and A_{CC} is grey. White space indicates zero entries. The corresponding m-SFI system is shown in (c), where light-green indicates matrix blocks that are zero in the m-SFI system, but are non-zero in the corresponding AI system. A first mixed parabolic-hyperbolic system is formed with all the pressure equations but only the composition equations of the first six cells and a second hyperbolic-only system is formed with the composition equations of the last four cells.

light-blue, , A_{CP} is green , and A_{CC} is grey. Figure 1b shows the corresponding system for the Adaptive Implicit (AI) method [15, 43] assuming that the last four gridblocks are treated using the IMPES method. In these representations, white space indicates zero coefficients. A detailed look at the figure 1b indicates that the AI-based system can be decomposed into two smaller systems: one independent system for the implicitly treated flow problems and one for the explicitly treated transport equations. The former sub-system, which is of mixed parabolic-hyperbolic type, can be solved using the Constrained Pressure Residual (CPR) approach [6] that employs an Algebraic Multi-Grid (AMG) solver for the pressure system [42]. Figure 1c shows the corresponding system for the proposed m-SFI method (30). In this figure, light-green indicates matrix blocks that are zero in m-SFI, but are non-zero in the corresponding AI system of figure 1b. The AMG-CPR solver can be used to deal with the sub-system obtained using the AI and m-SFI schemes. In our studies, we have observed practically the same number of linear-solver iterations for systems described by (28) and (30). Moreover, if mass transfer occurs in a small portion of the reservoir model, the cost of solving system (30) is equal to the cost of inverting an AI matrix with mainly IMPES-like cells, which is much cheaper than inverting system (28) of the FI method. After each pressure update, a phase-split algorithm is applied in order to change the phase-state and to check if the pressure has crossed the

bubble-point. We introduce the matrix I_c, which consists of zeros except for ones on the diagonal, where additional coupling terms are required. With this definition, the m-SFI component update can be described as follows:

$$\begin{aligned} &\text{compute } \delta P \text{ from a m-SFI pressure iteration} \\ &\delta C = A_{CC}^{-1} \cdot [R_C - I_c \cdot A_{CP} \cdot \delta P] \\ &C = C + \delta C. \end{aligned} \tag{32}$$

This component update entails a pressure system computation, a transport system computation, and a phase-split computation. The block-matrix A_{CC} is solved by GMRES preconditioned by Block Incomplete Lower-Upper factorization with zero fill-in (BILU(0)). We use the computed δP in regions where the additional coupling terms are needed for the transport system, and we keep the usual SFI transport system in regions where no additional coupling terms are required. This localization is expected to be very efficient in a multiscale framework. Note that two pressure systems and one component system are solved for each m-SFI iteration. There is not outer or inner iteration as for the conventional SFI method. The m-SFI method is described in algorithm 3.

compute R_P and R_C
while $max(|R_P|, |R_C|) > \epsilon$ **do**
  % pressure update
  compute A_{PP}, A_{PCR}, A_{CP} and A_{CCR}
  $\begin{pmatrix} A_{PP} & A_{PCR} \\ A_{CP} & A_{CCR} \end{pmatrix} \begin{pmatrix} \delta P \\ \delta C \end{pmatrix} = - \begin{pmatrix} R_P \\ R_C \end{pmatrix}$
  discard δC and update $P = P + \delta P$
  compute phase-split
  % saturation/compositions update
  compute A_{CC}
  recompute A_{PP}, A_{PCR}, A_{CP}, A_{CCR}, R_P and R_C
  % first step is to compute a δP
  $\begin{pmatrix} A_{PP} & A_{PCR} \\ A_{CP} & A_{CCR} \end{pmatrix} \begin{pmatrix} \delta P \\ \delta C \end{pmatrix} = - \begin{pmatrix} R_P \\ R_C \end{pmatrix}$
  discard δC and keep δP
  % saturation/compositions update with localized coupling
  $\delta C = A_{CC}^{-1} \cdot [R_C - I_c \cdot A_{CP} \cdot \delta P]$
  $C = C + \delta C$
  compute phase-split
  recompute R_P and R_C
end

Algorithm 3: m-SFI algorithm

The cost of one m-SFI iteration is equivalent to two AI matrix inversions, and one A_{CC} matrix inversion. The cost of solving the pressure system with AMG is given as $c_{AMG} = \alpha_{AMG}\, n_{cell} \log(n_{cell})$ with α_{AMG} a constant, and n_{cell} is the number of cells in the model. The cost of one BILU(0)-GMRES iteration is given as $c_{ILU} = \alpha_{ILU}\, n_z$ with α_{ILU} a constant, and n_z is the number of non-zero entries in the matrix. For the cases we tested, the FI and AI systems required the same number of CPR iterations, n_{CPR}. We observed that the essentially hyperbolic (transport) problem represented by the matrix A_{CC} requires less BILU(0)-GMRES iterations compared with the FI or AI formulations with CPR; that is, $\frac{n_{CPR}}{n_{ILU}} \in [1.2, 3]$, where n_{ILU} is the number of required BILU(0)-GMRES iterations. We introduce the number of non-zero block-entries, n_{bz}, for a block matrix (block structure of the matrix due to several equations and variables per cell), and the fraction c_{FI} of FI cells in the m-SFI iteration. For the FI update, the number of non-zero entries in the matrix is: $n_h^2\, n_{bz}$ with n_h the number of hydrocarbon components. For

the m-SFI pressure update, constructing the pressure system and ignoring the cross-terms at the boundary with the FI cells, the number of non-zero entries in the matrix is $(1 - c_{FI} + c_{FI} n_h^2)\, n_{bz}$. For the m-SFI composition update, the number of non-zero entries in the matrix is $(n_h - 1)^2\, n_{bz}$. The complexity ratio of one m-SFI iteration versus one FI iteration can be written as:

$$\frac{2\, n_{CPR} \left[\frac{c_{AMG}}{n_{bz}} + \alpha_{ILU}(1 - c_{FI} + c_{FI} n_h^2) \right] + n_{ILU} \alpha_{ILU} (n_h - 1)^2}{n_{CPR} \left[\frac{c_{AMG}}{n_{bz}} + \alpha_{ILU} n_h^2 \right]}. \tag{33}$$

If we only consider the cost of the AMG solver by setting α_{ILU} in equation (33) to zero, we observe twice as many AMG solves in one m-SFI iteration compared with one FI iteration. These AMG solves for the m-SFI method can be replaced by a multiscale method. Since the second pressure solution in m-SFI is required only in regions with mass transfer, we anticipate that it can potentially be obtained at a low computational cost. If we only look at the cost of the BILU(0)-GMRES iterations by setting c_{AMG} in equation (33) to zero, we obtain

$$\frac{2\, \frac{n_{CPR}}{n_{ILU}} (1 - c_{FI} + c_{FI} n_h^2) + (n_h - 1)^2}{\frac{n_{CPR}}{n_{ILU}} n_h^2}. \tag{34}$$

Figure 2 shows the cost ratio of BILU(0)-GMRES for one m-SFI iteration to one FI iteration for various coupling fractions c_{FI} with $n_h = 6$ and $n_h = 11$ hydrocarbon components and $\frac{n_{CPR}}{n_{ILU}} = 1.2$, 2 and 3. We see that the cost of the BILU(0)-GMRES part in one m-SFI iteration can be more than three times lower than for one FI iteration for the cases with $\frac{n_{CPR}}{n_{ILU}} = 3$, if the coupling fraction c_{FI} is kept close to zero. The m-SFI scheme for the cases with $\frac{n_{CPR}}{n_{ILU}} = 3$ are two times less expensive per iteration if $c_{FI} = 0.1$. For the cases with $\frac{n_{CPR}}{n_{ILU}} = 1.2$, 2 and 3, the c_{FI} values have to be smaller than approximately 0.18, 0.3 and 0.35, respectively, in order that one m-SFI iteration cheaper is than one FI iteration. The latter condition is expected to be applicable in practice, since usually much less than 20% of the cells in field-scale models would experience mass-transfer between the fluid phases during a given timestep. Moreover, in our numerical experiments it has been observed that the m-SFI sequential algorithm can outperform the FI method in terms of the required number of overall iterations, when gas appears or disappears. This is due to the local constraints representing the gas-oil phase

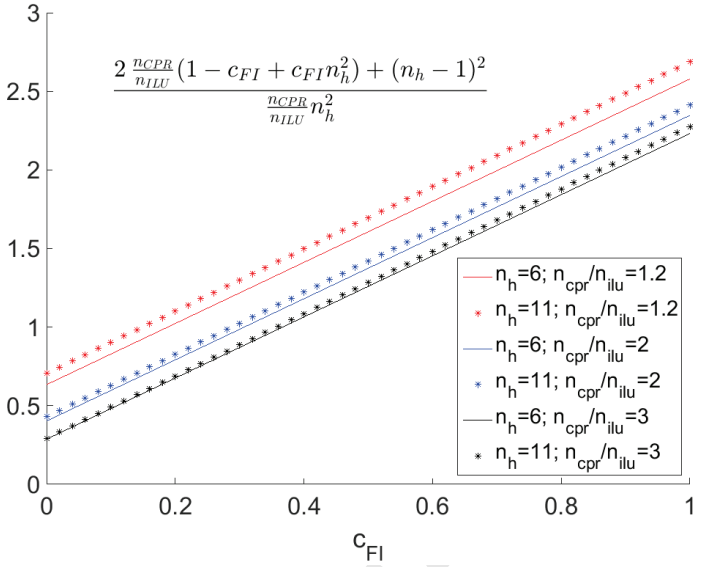

Figure 2: Cost ratio of BILU(0)-GMRES for one m-SFI iteration to that of one FI iteration for various coupling fractions c_{FI}, hydrocarbon components n_h and ratios $\frac{n_{CPR}}{n_{ILU}}$.

equilibrium, which are added, or removed, after each Newton iteration in the FI method based on the natural-variables formulation. For instance, if a model which is initially saturated with oil gets depleted during the first Newton iteration, the component updates in the FI method will not take into account the appearance of the gas phase. On the contrary, in the m-SFI iteration, the phase-split computations after the pressure update detect the change in the phase-state (appearance of gas), which is then taken into account during the component update. The scenario is similar for recompression. We believe this is the primary reason why the m-SFI method can converge in fewer iterations than the FI method.

Note that if A_{PCR} and A_{CCR} in the m-SFI algorithm are set to A_{PC} and A_{CC}, then the first pressure update is exactly the same as in the FI method. But then, only if the subsequent phase-split computations, Jacobian and residual updates are skipped, and if I_c is an identity matrix, the same component update as in the FI method is obtained. On the other hand, if A_{PCR} and A_{CP} are set to zero, then the m-SFI method is identical to one SFI pressure iteration followed by one SFI composition iteration. A variant of the m-SFI method would be to compute δP, and to update the compositions

with $\delta C = A_{CC}^{-1} \cdot (R_C - A_{CP} \cdot \delta P)$ without doing the phase-split computation. Based on our experience, however, this approach usually takes 2 to 3 times more iterations compared with the m-SFI algorithm presented above.

3. Numerical Experiments and Discussion

Numerical tests of the m-SFI algorithm were performed using a previously developed reservoir simulator [30, 31]. Four different fluids, and two different reservoir models are considered. The fluids are: (i) 2-hydrocarbon component fluid "2HC" with a K-value function of pressure for the mass exchange formulation; (ii) 11-hydrocarbon component fluid "11HC", also with pressure dependent K-values; (iii) the fluid model of the SPE comparative solution project 5 [23], "SPE5-0", with the Peng-Robinson cubic equations of state without the impact of composition on molar densities and viscosities (values taken for reference gas and oil compositions); (iv) the fluid "SPE5" of the full SPE comparative solution project 5 with correlations for the densities and viscosities. The models are: (a) homogeneous 1D model with 50 cells; (b) heterogeneous 2D model with 220×60 cells taken from the top layer of the SPE 10 problem [8]; the corresponding permeability field is shown in figure 3. More details on the numerical setups are given in Appendix A. In order to compare the different methods, an extremely tight convergence criterion was applied, i.e. a timestep is considered converged, if for each component and for each cell the relative material-balance error is smaller than 10^{-6}.

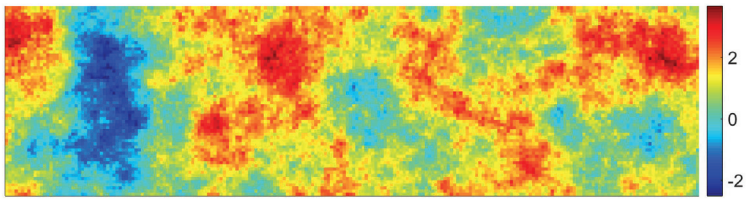

Figure 3: log10(K) field of the 2D model with 220×60 cells. Permeability unit is millidarcy.

In a first test series, the reservoirs are initially 100% filled with oil, and depletion occurs at the right boundary, where a low pressure (below bubble point) is applied; the other boundaries are impermeable. In this setting, the low pressure diffuses into the domain, and gas appears near the right boundary. Obviously, this phase-change is strongly coupled to the pressure

evolution. In a second test series, the two fluid phases are re-compressed by injecting at the right boundary. In addition to these depletion and recompression test cases, a more realistic 2D simulation study with the "SPE5"-fluid and the permeability field of figure 3 is presented. The light component is injected at the lower-left corner, and oil is produced at the upper-right corner; for this case it was found that the m-SFI convergence is similar to that of the FI method, and that it is consistently better than the convergence rates of the SFI and IMPES methods.

3.1. Depletion Test Cases

Figure 4 shows the gas-phase saturation profiles for the 1D 50-cell model after one depletion timestep, which is much larger than the timestep allowed for the IMPES algorithm (CFL limit). The results for the four different fluids are summarized in table 1. CFL_S is the CFL number for the explicit treatment of saturation, and CFL_X is the CFL number for the explicit treatment of compositions. The IMPES algorithm is stable, if both CFL_S and CFL_X are less than one [12]. The results show that the m-SFI method converges in the same number (or even less) iterations compared with the FI method. Note that FI coupling is only needed in the region where gas appears during the timestep. The SFI method does not converge for the cases with fluids "2HC" and "11HC"; therefore, the coupling terms in the gas region are critically important. The CFL_{SF} and CFL_{XF} numbers give an indication of the coupling strength between the pressure and the component transport equations. For these two test cases, even if these numbers are not extremely large during the last iterations, during the early iterations, the CFL_{SF} can reach values between 3000 and 5000 and the CFL_{XF} reaches 400. This strong coupling between the pressure and the transport due to interphase mass transfer has a very negative impact on the conventional SFI method. This motivated the development of the modified SFI scheme, whereby the additional coupling is accounted for in the construction of the pressure equation. As soon as the gas phase appears in the cases with the "2HC" and "11HC" fluids, the coupling between pressure and transport becomes so strong that overshoots appear in the SFI solutions. With these fluids, even with a reduced timestep size, the SFI method only converges as long as no gas appears. Unlike the cases with "2HC" and "11HC", the SFI method converges for the "SPE5-0" and "SPE5" fluids. For those two test cases, during all the SFI iterations, the CFL_{SF} and CFL_{XF} values remain below one, which reflects that the thermodynamic coupling is weak. With the "SPE5-0" and "SPE5" fluids, however,

Table 1: Depletion results for the 1D model with 50 cells. ∞ denotes non converging cases.

fluid	CFL_S / CFL_X	CFL_{SF}/ CFL_{XF}	initial/final cells with gas	FI coupling	FI iterations	m-SFI iterations	SFI iterations
2HC	3 / 4	0.9 / 1	0% / 46%	48%	7	4	∞
11HC	3 / 3	0.5 / 27	0% / 24%	78%	6	6	∞
SPE5-0	24 / 6	0.12 / 0.7	0% / 32%	46%	7	7	17
SPE5	21 / 5	0.17 / 1	0% / 36%	68%	10	15	31

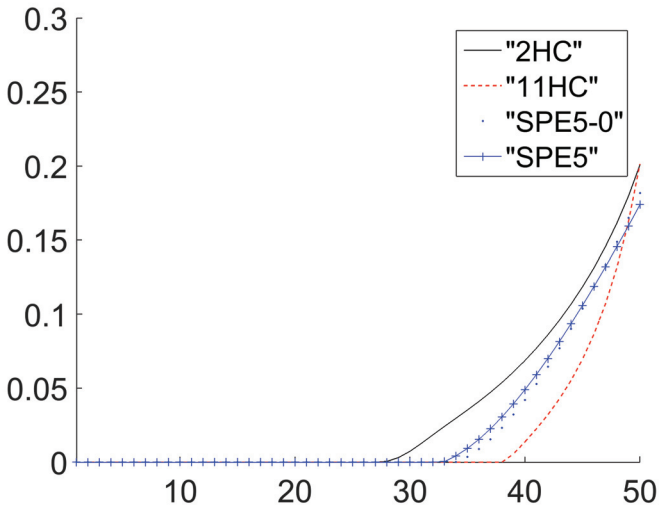

Figure 4: S_g profiles versus cell number for the 1D depletion test cases after one timestep.

17 and 31 SFI iterations are required, respectively, compared with 7 and 15 m-SFI iterations. In summary, for these 1D depletion test cases, the same timestep size can be chosen for the m-SFI method as for the FI method, and the convergence rates are similar (same or fewer number of iterations for the m-SFI method than for the FI method except "SPE5" requiring 1.5 times as many iterations). The IMPES method, on the other hand, requires much smaller timesteps, and the SFI method either does not converge at all, or requires up to 2.4 times more iterations than the m-SFI method.

The same depletion scenario was studied for the 2D model with 220×60 cells; the results are summarized in table 2. Figures 5a, 5b, 5c and 5d show the gas saturation profiles after one timestep; starting with 100% oil in the whole reservoir. From table 2 it can be seen that the m-SFI method is stable for very large CFL numbers. Since the density and viscosity of the "SPE5-0"

Table 2: Depletion results for the 2D model with 220×60 cells. The asterisk denotes the use of another version of the m-SFI method where δP is not localized for the δC update and ∞ denotes non converging cases.

fluid	CFL_S/ CFL_X	CFL_{SF}/ CFL_{XF}	initial/final cells with gas	FI coupling	FI iterations	m-SFI iterations	SFI iterations
2HC	55 / 180	29 / 2.3	0% / 33%	37%	8	7	∞
11HC	125 / 140	1 / 1771	0% / 19%	45%	8	7	∞
SPE5-0	500 / 140	1 / 1	0% / 16%	19%	24	8	∞
SPE5	450 / 125	1 / 1.4	0% / 17%	41%*	10	10*	∞

fluid do not depend on composition, a smaller number of cells require FI coupling compared to the case with the "SPE5" fluid. The m-SFI method converges in almost the same number of iterations as the FI method, while the SFI method does not converge in either case. For example, with the "SPE5-0" fluid the m-SFI method converges in 8 iterations, whereas the FI method requires 24 iterations. For the "SPE5" fluid, another version of the m-SFI method had to be used in order to achieve convergence: in many oil-only cells, the impact of composition change on pressure is large, and the SFI assumption for the composition update is too strong. While the presented m-SFI method does not converge in this case, convergence is achieved, if we do not localize δP for the δC update in equation (32), in which case I_c is the identity matrix. With this modification, convergence was achieved in 10 iterations with 41% of cells requiring FI coupling. In practice, this modification is not used.

For the above test cases, neither capillarity pressure nor gravity have been considered. The simulation runs were repeated with small and large capillary-pressure and gravity effects. Again very similar convergence properties have been observed for the m-SFI and FI methods. However, due to the stronger coupling between flow and transport, more cells require FI treatment in the m-SFI method. The m-SFI method is advantageous, since its convergence properties are comparable to those of the FI method at a cost per iteration closer to that of an SFI iteration.

3.2. Re-Compression Test Cases

We consider challenging cases in which recompression from 100% gas to 100% oil takes place in two timesteps. This is achieved by applying a high-pressure value at the right boundary. Note that for all four fluids this creates extremely challenging problems with shocks and huge CFL numbers.

Table 3 and figure 6 show the results for the second timestep with the

(a) "2HC" fluid

(b) "11HC" fluid

(c) "SPE5-0" fluid

(d) "SPE5" fluid

Figure 5: S_g maps for the 2D depletion test cases after one timestep.

Table 3: Recompression results for the 1D model with 50 cells. ∞ denotes non converging cases.

fluid	CFL_S/ CFL_X	CFL_{SF}/ CFL_{XF}	initial/final cells with gas	FI coupling	FI iterations	m-SFI iterations	SFI iterations
2HC	100 / 1.2	0.97 / 0.98	66% / 0%	68%	7	6	∞
11HC	520 / 7	1 / 264	54% / 0%	56%	12	9	∞
SPE5-0	70 / 5	0.98 / 1	68% / 0%	70%	12	10	∞
SPE5	100 / 5	0.98 / 1.09	72% / 32%	74%	12	10	∞

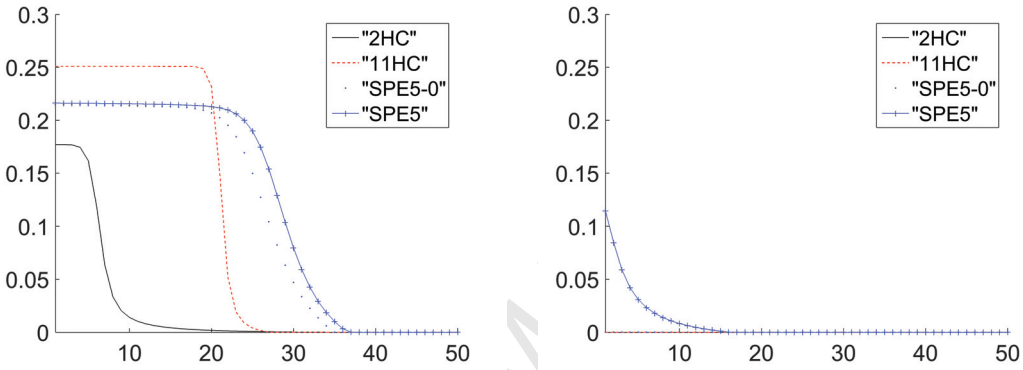

Figure 6: S_g profiles versus cell number for the 1D recompression test cases at the beginning (left) and at the end (right) of the second timestep.

1D model. The fraction of cells with FI coupling cannot be smaller than the maximum percentage of cells with gas during the timestep. For all the test cases, this fraction is close to optimal, and the m-SFI method converges in fewer iterations that the FI method. Note that for all these test cases the (standard) SFI method does not converge, even if the timestep size is reduced dramatically.

The same two-step recompression process was performed for the 2D 220×60 model. The results are summarized in table 4 and figures 7 and 8. With the fluids "2HC", "11HC" and "SPE5-0", the m-SFI method works well; that is, it converges in about the same number of iterations as the FI method with FI coupling in only those cells with gas and all in situations where SFI does not converge. For the "SPE5" fluid case, 25% more iterations are necessary with the m-SFI method compared with the FI method. As in the 1D test cases, the SFI method does not converge for any of the four 2D cases. Based on our investigations, we conclude that the m-SFI method is a very promising sequential-implict solution strategy with convergence behavior comparable

Table 4: Recompression results for the 2D model with 220×60 cells. ∞ denotes non converging cases.

fluid	CFL_S/ CFL_X	CFL_{SF}/ CFL_{XF}	initial/final cells with gas	FI coupling	FI iterations	m-SFI iterations	SFI iterations
2HC	8500 / 90	18 / 7	74% / 0%	75%	9	10	∞
11HC	10000 / 140	15 / 52	60% / 13%	60%	17	16	∞
SPE5-0	1050 / 85	1 / 1	63% / 16%	65%	27	31	∞
SPE5	1450 / 75	1 / 1	66% / 18%	68%	15	20	∞

to the FI method.

3.3. Realistic Case

Here, assessment of the m-SFI method for a more realistic scenario is presented. The light component of the "SPE5" fluid is injected at the lower-left corner of the SPE 10 top layer model depicted in figure 3, and oil is produced from the upper-right corner. Initially, the entire reservoir is saturated with oil, and at the end of the simulation 16% of the domain contains gas. A standard heuristic rule is employed for time stepping, i.e., the timestep size is chosen such that the maximum saturation change is close to 0.2. The FI method requires 77 timesteps with an average of 3.8 Newton iterations. The average maximum CFL_S and CFL_X values per timestep are 39 and 72, respectively, with maximum values of 206 and 236. The maximum CFL_{SF} and CFL_{XF} values per timestep have averages of 3350 and 15300, respectively, with maximum values of 6e4 and 4e5. The final gas saturation is shown in figure 9. If the SFI method is used for this test case, the nonlinearities due to interphase mass transfer are so severe that the method requires timesteps that are up to 1000 times smaller to converge. With the m-SFI method, on the other hand, convergence is achieved in 88 timesteps, which is close to the 77 timesteps required by the FI method. With an average of 5.5 iterations per timestep and an average of 7% FI coupling, the m-SFI method is more efficient than the FI method. Note that this scenario and behavior are expected to be representative of practical compositional simulation studies. The m-SFI and FI methods have similar convergence properties, while many more Newton iterations and smaller timesteps are required by the SFI method.

4. Conclusions

A modified SFI method is proposed, in which the SFI operator is complemented with local approximations of the coupling terms between pressure and

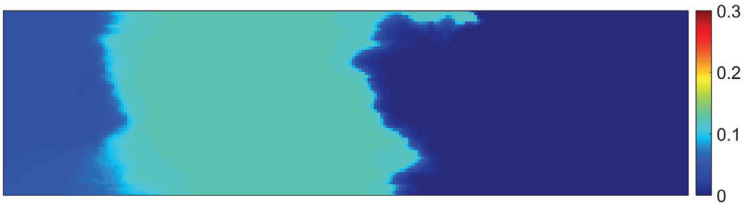

(a) "2HC" fluid at beginning of timestep

(b) "2HC" fluid at end of timestep

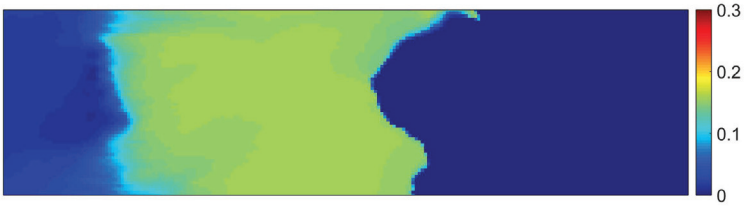

(c) "11HC" fluid at beginning of timestep

(d) "11HC" fluid at end of timestep

Figure 7: S_g maps for the 2D recompression test cases with the fluids "2HC" and "11HC".

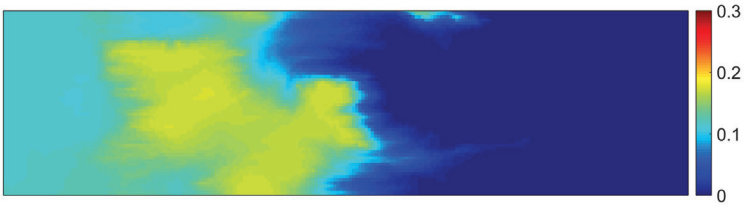

(a) "SPE5-0" fluid at beginning of timestep

(b) "SPE5-0" fluid at end of timestep

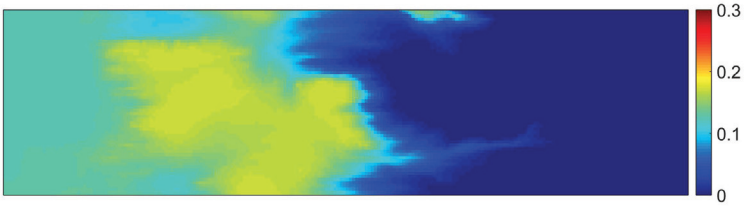

(c) "SPE5" fluid at beginning of timestep

(d) "SPE5" fluid at end of timestep

Figure 8: S_g maps for the 2D recompression test cases with the fluids "SPE5-0" and "SPE5".

Figure 9: Gas saturation at the end of the simulation (some blue pixels are due to inactive cells)

transport. This method decouples the mixed parabolic/hyperbolic problem into a parabolic pressure equation with some contributions from the cells with mass transfer between the fluid phases. The hyperbolic transport equations in the second stage remain unchanged. The method was tested using one and two dimensional depletion and recompression test cases with two, six, and eleven-component fluids; both K-values and EOS-based formulations were employed. We show that the m-SFI method converges for problems where the coupling is too strong for the standard SFI scheme to converge. More importantly, we show that the m-SFI algorithm has convergence properties that are similar to those of the FI method across the wide parameter range investigated. Thus, we strongly recommend using the m-SFI method for sequential formulations, in general, and multiscale formulations (e.g., MSFV) in particular.

5. Nomenclature

- ϕ porosity of the rock
- K permeability in mD
- D depth in ft
- g gravitational acceleration in ft^2-Psi/lb
- n_h number of hydrocarbon components
- MW_c molar fraction of component c
- P_p pressure of phase p in Psi
- $P_c(S_g) = P_g - P_o$ capillary pressure in Psi

- S_g and S_o gas and oil saturations ($S_o = 1 - S_g$)
- x_c mass fraction of component c in the oil phase
- y_c mass fraction of component c in the gas phase
- z_c global mass fraction of component c
- ρ_p phase mass density in lb/ft^3
- μ_p phase dynamic viscosity in cP
- k_{r_p} relative permeability for phase p
- K_c K-value of hydrocarbon component c between gas and oil phases
- $\hat{f}_{c,p}$ fugacity of hydrocarbon component c in phase p in Psi
- u_p velocity of phase p in ft/day
- u_t total velocity in ft/day
- f_p fractional flow for phase p
- λ_p mobility for phase p in cP^{-1}
- λ_t total mobility in cP^{-1}
- q_c and q well contributions (source or sink) in lb/day

6. Acknowledgments

The authors would like to thank TOTAL management for permission to publish this work.

7. Appendix A: Description of the Models

The three models used in this study have all cell dimensions of $dx = 20$ ft, $dy = 10$ ft, $dz = 2$ ft. The 50-cell model has gravity in the first dimension (when tested) and has constant porosity $\phi = 0.35$ and constant permeability $K = 100$ mD. The 220×60-cell model has gravity in the first dimension (when tested), has constant porosity $\phi = 0.35$, but has its permeability K from the top layer of SPE 10 comparative solution project [8]. The realistic

Table 5: Component molecular weights for "11HC" fluid in lb/lbmol.

C_1	C_2	C_3	C_4	C_5	C_6	C_7	C_8	C_9	C_{10}	C_{11}
16.04	30.07	44.1	58.12	72.15	90.86	111	147.4	192	240.08	387.16

model has 220×60 cells with porosity and permeabilities from the top layer of SPE 10.

The rock compressibility for all test cases is 1.78e-5 1/Psi. The relative permeabilities are linear for both the oil and the gas phases. The capillary pressure is usually zero, unless specified. In this second case, a very large non-physical value of $P_{c_{max}} = 50.0$ Psi with the expression $P_c = P_g - P_o = S_g \cdot P_{c_{max}}$ is used.

The component molecular weights for fluid "2HC" are 25.0 lb/lbmol and 50.0 lb/lbmol and are given in table 5 for fluid "11HC". For fluids "SPE5-0" and "SPE5" we refer the reader to [23]. The gas mass densities for the fluids "2HC", "11HC" and "SPE5-0" are given as

$$\rho_g = MW_g \frac{P}{0.96RT}, \tag{35}$$

where MW_g is the molecular weight of the gas phase, R is the ideal gas constant and T is the temperature. The gas viscosities for the fluids "2HC", "11HC" and "SPE5-0" are given by the CMG-STARS [9] correlation (T in °F, μ_g in cP)

$$\mu_g = 0.0136 + 2.111e-5\,T. \tag{36}$$

The oil mass densities for the fluids "2HC", "11HC" and "SPE5-0" are given as:

$$\rho_o = \frac{\rho^{ref}}{1 - C_P(P - P_{initial})}, \tag{37}$$

where ρ^{ref} is a reference density, C_P the compressibility and $P_{initial}$ the pressure at the initial state. For "2HC", ρ^{ref} in lb/ft^3 is a function of the composition; that is,

$$\frac{1}{\rho^{ref}} = \frac{x_L}{25.0} + \frac{x_H}{62.0}, \tag{38}$$

whereas for "11HC" and "SPE5-0", ρ^{ref} is fixed at 52.0 lb/ft^3 and 35.5 lb/ft^3, respectively. The oil phase compressibility C_P is 5.0e-6 1/Psi for the "2HC" and "11HC" fluids and 2.5e-5 1/Psi for the "SPE5-0" fluid. The oil viscosities for "2HC", "11HC" and "SPE5-0" are constant and their values

Table 6: Component K-values for the "2HC" fluid.

	C_L	C_H
A	0.0	0.0
B	49012.0	0.0
C	0.0	0.0
D	1616.22	0.0
E	-446.78	0.0

Table 7: Component K-values for the "11HC" fluid.

	C_1	C_2	C_3	C_4	C_5	C_6
A	0.5854	1.621	2.952	4.754	7.934	14.56
B	4651	4884	5833	7198	9792	15360
C	$4.9\ 10^{-5}$	0.0001653	0.0005153	0.001275	0.003337	0.01077
D	34.13	513.4	1055	1618	2338	3402
E	7.263	-143.17	-214.57	-256.37	-289.27	-322.57

	C_7	C_8	C_9	C_{10}	C_{11}
A	21.59	27.76	90.62	-966.8	147500
B	22310	48860	143800	47210	-19380000
C	0.02597	0.1234	0.6199	3.148	163.4
D	4337	5978	8036	9814	16090
E	-345.77	-367.75	-383.43	-393.22	-403.24

are 1.3 cP, 1.3 cP and 0.2 cP, respectively. Phase-split is modelled for "2HC" and "11HC" by the Crookston correlation K-values (with P in Psi, T in °F)

$$K_c(P,T) = (A + B/P + CP)e^{\frac{-D}{T-E}} \tag{39}$$

for each components. The numerical values for "2HC" and "11HC" are given in tables 6 and 7. The "SPE5" fluid uses the Peng-Robinson equation of state [36] for density and phase-split calculations, as well as the Lorentz-Bray-Clark [27] method for the viscosity [23]. "SPE5-0" uses the Peng-Robinson equation of state only for the phase-split calculation.

The test cases with fluid "2HC" have initial conditions with $P = 500.0$ Psi, $T = 60$°F, $S_o = 1.0$ and $x_L = 0.2$. The test cases with fluid "11HC" have initial conditions with $P = 1100.0$ Psi, $T = 250$°F and $S_o = 1.0$; table 8 provides the composition values. The test cases with fluids "SPE5-0" and "SPE5" have initial conditions with $P = 4000.0$ Psi, $T = 160$°F and $S_o = 1.0$; table 9 provides the composition values. The connection factors for all the cell-well connections are fixed at 0.3 Rbbl.cP/day-Psi. The fluids "2HC",

Table 8: Initial oil composition for "11HC" fluid.

C_1	C_2	C_3	C_4	C_5	C_6	C_7	C_8	C_9	C_{10}	C_{11}
0.1890	0.0630	0.0315	0.0504	0.0441	0.0441	0.0441	0.0630	0.0567	0.0819	0.3322

Table 9: Initial oil composition for "SPE5-0" and "SPE5" fluids.

C_1	C_2	C_3	C_4	C_5	C_6
0.5	0.03	0.07	0.2	0.15	0.05

"11HC", "SPE5-0" and "SPE5" are produced respectively at 150 Psi, 500 Psi, 1800 Psi and 1800 Psi during the depletion and then the produced fluids are re-injected. In the realistic test case with fluid "SPE5", 6 Mscf/day of the first hydrocarbon component are injected and production occurs at 4000 Psi.

8. Appendix B: Stability Analysis

For the following stability analysis we consider the saturation transport equation

$$\frac{\partial S}{\partial t} = -a_t \frac{\partial S}{\partial x} + d\frac{\partial^2 S}{\partial x^2} - a_f \frac{\partial S}{\partial x}. \tag{40}$$

We derive the CFL number for the explicit treatment of the thermodynamics by considering the implicit treatment of the terms $a_t \frac{\partial S}{\partial x}$ and $d\frac{\partial^2 S}{\partial x^2}$ and the explicit treatment of $a_f \frac{\partial S}{\partial x}$. Time derivatives are approximated by as Euler scheme; first-order spatial derivatives are discretized using single-point upstream weighting (assuming positive a_t and a_f values) and second-order spatial derivatives are discretized with a central scheme:

$$\frac{\partial S}{\partial t} = \frac{S_x^{t+\delta t} - S_x^t}{\delta t} = \Delta_t S, \tag{41}$$

$$\frac{\partial S^*}{\partial x} = \frac{S_x^* - S_{x-\delta x}^*}{\delta x} = \Delta_x S^* \tag{42}$$

$$\text{and } \frac{\partial^2 S^*}{\partial x^2} = \frac{S_{x+\delta x}^* - 2S_x^* + S_{x-\delta x}^*}{\delta x^2} = \Delta_{xx} S^*. \tag{43}$$

We then obtain the discretized equation

$$\Delta_t S = -a_t \Delta_x S^{t+\delta t} + d\Delta_{xx} S^{t+\delta t} - a_f \Delta_x S^t. \tag{44}$$

Without taking into account boundary conditions, stability can be investigated with a Neumann analysis. Therefore a spectral representation of the error is considered, where one mode at time t associated with the wavenumber β reads

$$\xi_S(x,t) = \xi^t e^{-j\beta x} \tag{45}$$

Since (44) also holds for each error mode, one obtains

$$\frac{\xi^{t+\delta t}-\xi^{t}}{\delta t}+a_t\frac{1-e^{-j\beta\delta x}}{\delta x}\xi^{t+\delta t}+2d\frac{1-\cos\left(\beta\delta x\right)}{\delta x^2}\xi^{t+\delta t}+a_f\frac{1-e^{-j\beta\delta x}}{\delta x}\xi^{t}=0 \tag{46}$$

and then

$$\frac{\xi^{t+\delta t}}{\xi^{t}}=\frac{1-a_f\frac{\delta t}{\delta x}\left(1-e^{-j\beta\delta x}\right)}{1+a_t\frac{\delta t}{\delta x}\left(1-e^{-j\beta\delta x}\right)+2d\frac{\delta t}{\delta x^2}\left(1-\cos\left(\beta\delta x\right)\right)}=M_\beta^{\delta t} \tag{47}$$

for the amplification factor of the mode. The stability condition is that $|M_\beta^{\delta t}|<1$ for every wavenumber β. While the maximum amplification factor is not always reached at $\beta=\frac{\pi}{\delta x}$, in practice using $\beta=\frac{\pi}{\delta x}$ gives a good estimate. The CFL number is then defined as

$$CFL_{SF}=\left|\frac{2a_f\frac{\delta t}{\delta x}-1}{2a_t\frac{\delta t}{\delta x}+4d\frac{\delta t}{\delta x^2}+1}\right|. \tag{48}$$

The usual CFL number for the explicit treatment of saturation is derived by considering the explicit treatment of the terms $a_t\frac{\partial S}{\partial x}$ and $d\frac{\partial^2 S}{\partial x^2}$ and by ignoring $a_f\frac{\partial S}{\partial x}$. One obtains as stability condition

$$\left|2a_t\frac{\delta t}{\delta x}+4d\frac{\delta t}{\delta x^2}-1\right|<1 \tag{49}$$

but in practice, $2a_t\frac{\delta t}{\delta x}+4d\frac{\delta t}{\delta x^2}$ is real and positive, resulting in the equivalent criterion

$$CFL_S=\delta t\left|a_t\frac{1}{\delta x}+2d\frac{1}{\delta x^2}\right|<1. \tag{50}$$

9. Appendix C: SI Metric Conversion Factors

1	Psi	=	100000/14.5037	Pa
1	ft	=	1/3.2808	m
1	lb	=	1/2.20462262	kg
1	mD	=	9.869e-16	m^2
1	cP	=	0.001	Pa.s
1	day	=	86400	s

10. References

[1] J.E. Aarnes. On the use of a mixed multiscale finite element method for greater flexibility and increased speed or improved accuracy in reservoir simulation. *Multiscale Modeling & Simulation*, 2(3):421–439, jan 2004. doi: 10.1137/030600655. URL http://dx.doi.org/10.1137/030600655.

[2] G. Acs, S. Doleschall, and E. Farkas. General purpose compositional model. *Society of Petroleum Engineers Journal*, 25(04):543–553, aug 1985. doi: 10.2118/10515-pa. URL http://dx.doi.org/10.2118/10515-PA.

[3] T. Arbogast and S.L. Bryant. A two-scale numerical subgrid technique for waterflood simulations. *SPE Journal*, 7(04):446–457, dec 2002. doi: 10.2118/81909-pa. URL http://dx.doi.org/10.2118/81909-PA.

[4] K. Aziz and A. Settari. *Petroleum Reservoir Simulation*. Applied Science Publishers, 1979.

[5] K. Aziz and T.W. Wong. Considerations in the development of multipurpose reservoir simulation models. *Proceedings of 1st and 2nd International Forum on Reservoir Simulation, Alpbach, Austria, Sept 12-16 1988 and Sept 4-8 1989*, September 1989.

[6] H. Cao, H.A. Tchelepi, J. Wallis, and H. Yardumian. Parallel scalable unstructured CPR-type linear solver for reservoir simulation. In *SPE Annual Technical Conference and Exhibition*. Society of Petroleum Engineers (SPE), 2005. doi: 10.2118/96809-ms. URL http://dx.doi.org/10.2118/96809-MS.

[7] Z. Chen and T.Y. Hou. A mixed multiscale finite element method for elliptic problems with oscillating coefficients. *Mathematics of Computation*, 72(242):541–577, jun 2002. doi: 10.1090/s0025-5718-02-01441-2. URL http://dx.doi.org/10.1090/S0025-5718-02-01441-2.

[8] M.A. Christie and M.J. Blunt. Tenth SPE comparative solution project: A comparison of upscaling techniques. *SPE Reservoir Evaluation & Engineering*, 4(04):308–317, aug 2001. doi: 10.2118/72469-pa. URL http://dx.doi.org/10.2118/72469-PA.

[9] CMG-STARS. Computer Modeling Group, Calgary, Alberta, Canada, 2004.

[10] K.H. Coats. An equation of state compositional model. *Society of Petroleum Engineers Journal*, 20(05):363–376, oct 1980. doi: 10.2118/8284-pa. URL http://dx.doi.org/10.2118/8284-PA.

[11] K.H. Coats. A note on IMPES and some IMPES-based simulation models. *SPE Journal*, 5(03):245–251, sep 2000. doi: 10.2118/65092-pa. URL http://dx.doi.org/10.2118/65092-PA.

[12] K.H. Coats. IMPES stability: Selection of stable timesteps. *SPE Journal*, 8(02):181–187, jun 2003. doi: 10.2118/84924-pa. URL http://dx.doi.org/10.2118/84924-PA.

[13] K.H. Coats. IMPES stability: The CFL limit. *SPE Journal*, 8(03):291–297, sep 2003. doi: 10.2118/85956-pa. URL http://dx.doi.org/10.2118/85956-PA.

[14] R.B. Crookston, W.E. Culham, and W.H. Chen. A numerical simulation model for thermal recovery processes. *Society of Petroleum Engineers Journal*, 19(01):37–58, feb 1979. doi: 10.2118/6724-pa. URL http://dx.doi.org/10.2118/6724-PA.

[15] P.A. Forsyth and P.H. Sammon. Practical considerations for adaptive implicit methods in reservoir simulation. *Journal of Computational Physics*, 62(2):265 – 281, 1986. ISSN 0021-9991. doi: http://dx.doi.org/10.1016/0021-9991(86)90127-0. URL http://www.sciencedirect.com/science/article/pii/0021999186901270.

[16] L.T. Fussell and D.D. Fussell. An iterative technique for compositional reservoir models. *Society of Petroleum Engineers Journal*, 19(04):211–220, aug 1979. doi: 10.2118/6891-pa. URL http://dx.doi.org/10.2118/6891-PA.

[17] H. Hajibeygi and H.A. Tchelepi. Compositional multiscale finite-volume formulation. *SPE Journal*, 19(02):316–326, apr 2014. doi: 10.2118/163664-pa. URL http://dx.doi.org/10.2118/163664-PA.

[18] T.Y. Hou and X.-H. Wu. A multiscale finite element method for elliptic problems in composite materials and porous media.

Journal of Computational Physics, 134(1):169 – 189, 1997. ISSN 0021-9991. doi: http://dx.doi.org/10.1006/jcph.1997.5682. URL http://www.sciencedirect.com/science/article/pii/S0021999197956825.

[19] P Jenny, S.H. Lee, and H.A. Tchelepi. Multi-scale finite-volume method for elliptic problems in subsurface flow simulation. *Journal of Computational Physics*, 187(1):47 – 67, 2003. ISSN 0021-9991. doi: http://dx.doi.org/10.1016/S0021-9991(03)00075-5. URL http://www.sciencedirect.com/science/article/pii/S0021999103000755.

[20] P. Jenny, S.H. Lee, and H.A. Tchelepi. Adaptive fully implicit multi-scale finite-volume method for multi-phase flow and transport in heterogeneous porous media. *Journal of Computational Physics*, 217(2):627 – 641, 2006. ISSN 0021-9991. doi: http://dx.doi.org/10.1016/j.jcp.2006.01.028. URL http://www.sciencedirect.com/science/article/pii/S002199910600026X.

[21] H. Kazemi, C.R. Vestal, and D.G. Shank. An efficient multicomponent numerical simulator. *Society of Petroleum Engineers Journal*, 18(05):355–368, oct 1978. doi: 10.2118/6890-pa. URL http://dx.doi.org/10.2118/6890-PA.

[22] R.P. Kendall, G.O. Morrell, D.W. Peaceman, W.J. Silliman, and J.W. Watts. Development of a multiple application reservoir simulator for use on a vector computer. In *Middle East Oil Technical Conference and Exhibition*. Society of Petroleum Engineers (SPE), 1983. doi: 10.2118/11483-ms. URL http://dx.doi.org/10.2118/11483-MS.

[23] J. E. Killough and C. A. Kossack. Fifth comparative solution project: Evaluation of miscible flood simulators. In *SPE Symposium on Reservoir Simulation*. Society of Petroleum Engineers (SPE), 1987. doi: 10.2118/16000-ms. URL http://dx.doi.org/10.2118/16000-MS.

[24] S.H. Lee, C. Wolfsteiner, and H.A. Tchelepi. Multiscale finite-volume formulation for multiphase flow in porous media: black oil formulation of compressible, three-phase flow with gravity. *Computational Geosciences*, 12(3):351–366, 2008. ISSN 1420-0597. doi: 10.1007/s10596-007-9069-3. URL http://dx.doi.org/10.1007/s10596-007-9069-3.

[25] B. Li, Z. Chen, and G. Huan. The sequential method for the black-oil reservoir simulation on unstructured grids. *Journal of Computational Physics*, 192(1):36 – 72, 2003. ISSN 0021-9991. doi: http://dx.doi.org/10.1016/S0021-9991(03)00346-2. URL http://www.sciencedirect.com/science/article/pii/S0021999103003462.

[26] K.-A. Lie, O. Møyner, J.R. Natvig, A. Kozlova, K. Bratvedt, S. Watanabe, and Z. Li. Successful application of multiscale methods in a real reservoir simulator environment. In *15th European Conference on the Mathematics of Oil Recovery 2016 (ECMOR XV)*. European Association of Geoscientists & Engineers (EAGE), aug 2016. doi: 10.3997/2214-4609.201601893. URL http://dx.doi.org/10.3997/2214-4609.201601893.

[27] J. Lorentz, B.G. Bray, and C.R. Clark. Calculating viscosities of reservoir fluids from their compositions. *Journal of Petroleum Technology*, 16(10):1171–1176, oct 1964. doi: 10.2118/915-pa. URL http://dx.doi.org/10.2118/915-PA.

[28] R.C. MacDonald. Methods for numerical simulation of water and gas coning. *Society of Petroleum Engineers Journal*, 10(04):425–436, dec 1970. doi: 10.2118/2796-pa. URL http://dx.doi.org/10.2118/2796-PA.

[29] J.J. Martin. Cubic equations of state-which? *Industrial & Engineering Chemistry Fundamentals*, 18(2): 81–97, may 1979. doi: 10.1021/i160070a001. URL http://dx.doi.org/10.1021/i160070a001.

[30] A. Moncorgé and H.A. Tchelepi. Stability criteria for thermal adaptive implicit compositional flows. *SPE Journal*, 14(02):311–322, jun 2009. doi: 10.2118/111610-pa. URL http://dx.doi.org/10.2118/111610-PA.

[31] A. Moncorgé, L. Patacchini, and R. de Loubens. Multi-phase, multi-component simulation framework for advanced recovery mechanisms. In *Abu Dhabi International Petroleum Conference and Exhibition*. Society of Petroleum Engineers (SPE), 2012. doi: 10.2118/161615-ms. URL http://dx.doi.org/10.2118/161615-MS.

[32] O. Møyner and K.-A. Lie. A multiscale restriction-smoothed basis method for high contrast porous media represented on unstructured grids. *Journal of Computational Physics*, 304:46 – 71, 2016. ISSN 0021-9991. doi: http://dx.doi.org/10.1016/j.jcp.2015.10.010. URL http://www.sciencedirect.com/science/article/pii/S0021999115006725.

[33] O. Møyner and K.-A. Lie. A multiscale restriction-smoothed basis method for compressible black-oil models. *SPE Journal*, 21(06):2079–2096, dec 2016. doi: 10.2118/173265-PA. URL http://dx.doi.org/10.2118/173265-PA.

[34] L.X. Nghiem, D.K. Fong, and K. Aziz. Compositional modeling with an equation of state (includes associated papers 10894 and 10903). *Society of Petroleum Engineers Journal*, 21(06):687–698, dec 1981. doi: 10.2118/9306-pa. URL http://dx.doi.org/10.2118/9306-PA.

[35] J.S. Nolen and D.W. Berry. Tests of the stability and time-step sensitivity of semi-implicit reservoir stimulation techniques. *Society of Petroleum Engineers Journal*, 12(03):253–266, jun 1972. doi: 10.2118/2981-pa. URL http://dx.doi.org/10.2118/2981-PA.

[36] D.-Y. Peng and D.B. Robinson. A new two-constant equation of state. *Industrial & Engineering Chemistry Fundamentals*, 15(1):59–64, feb 1976. doi: 10.1021/i160057a011. URL http://dx.doi.org/10.1021/i160057a011.

[37] O. Redlich and J. N. S. Kwong. On the Thermodynamics of Solutions. V. An Equation of State. Fugacities of Gaseous Solutions. *Chemical Reviews*, 44(1):233–244, feb 1949. doi: 10.1021/cr60137a013. URL http://dx.doi.org/10.1021/cr60137a013.

[38] J.W. Sheldon, B. Zondek, and W.T. Cardwell. One-dimensional, incompressible, noncapillary two-phase fluid flow in porous media. *Trans AIME*, (216):290–296, 1959.

[39] G. Soave. Equilibrium constants from a modified Redlich-Kwong equation of state. *Chemical Engineering Science*, 27(6):1197–1203, jun 1972. doi: 10.1016/0009-2509(72)80096-4. URL http://dx.doi.org/10.1016/0009-2509(72)80096-4.

[40] A.G. Spillette, J.G. Hillestad, and H.L. Stone. A high-stability sequential solution approach to reservoir simulation. In *Fall Meeting of the Society of Petroleum Engineers of AIME*. Society of Petroleum Engineers (SPE), 1973. doi: 10.2118/4542-ms. URL http://dx.doi.org/10.2118/4542-MS.

[41] H.L. Stone and A.O. Stone. Analysis of gas-cap or dissolved-gas drive reservoirs. *Society of Petroleum Engineers Journal*, 1(02):92–104, jun 1961. doi: 10.2118/1518-g. URL http://dx.doi.org/10.2118/1518-G.

[42] K. Stueben. An introduction to algebraic multigrid. *Appendix in book "Multigrid" by U. Trottenberg, C.W. Oosterlee and A. Schueller, Academic Press*, pages 413–532, 2001.

[43] G.W. Thomas and D.H. Thurnau. Reservoir simulation using an adaptive implicit method. *Society of Petroleum Engineers Journal*, 23(05):759–768, oct 1983. doi: 10.2118/10120-pa. URL http://dx.doi.org/10.2118/10120-PA.

[44] D.V. Voskov and H.A. Tchelepi. Comparison of nonlinear formulations for two-phase multi-component EoS based simulation. *Journal of Petroleum Science and Engineering*, 82-83:101 – 111, 2012. ISSN 0920-4105. doi: http://dx.doi.org/10.1016/j.petrol.2011.10.012. URL http://www.sciencedirect.com/science/article/pii/S0920410511002683.

[45] J.W. Watts. A compositional formulation of the pressure and saturation equations. *SPE Reservoir Engineering*, 1(03):243–252, may 1986. doi: 10.2118/12244-pa. URL http://dx.doi.org/10.2118/12244-PA.

[46] L.C. Young and R.E. Stephenson. A generalized compositional approach for reservoir simulation. *Society of Petroleum Engineers Journal*, 23(05):727–742, oct 1983. doi: 10.2118/10516-pa. URL http://dx.doi.org/10.2118/10516-PA.

[47] H. Zhou, S.H. Lee, and H.A. Tchelepi. Multiscale finite-volume formulation for saturation equations. *SPE Journal*, 17 (01):198–211, mar 2012. doi: 10.2118/119183-pa. URL http://dx.doi.org/10.2118/119183-PA.